Available online at www.sciencedirect.com
SCIENCE DIRECT®
Journal of Power Sources 140 (2005) 392–399
JOURNAL OF POWER SOURCES
www.elsevier.com/locate/jpowsour

Model for energy conversion in renewable energy system with hydrogen storage

S. Kélouwani, K. Agbossou*, R. Chahine

Institut de recherche sur l'hydrogène, Université du Québec à Trois-Rivières, P.O. Box 500, Trois-Rivières, Qué., Canada G9A 5H7

Received 15 July 2004; accepted 16 August 2004
Available online 6 October 2004

Abstract

A dynamic model for a stand-alone renewable energy system with hydrogen storage (RESHS) is developed. In this system, surplus energy available from a photovoltaic array and a wind turbine generator is stored in the form of hydrogen, produced via an electrolyzer. When the energy production from the wind turbine and the photovoltaic array is not enough to meet the load demand, the stored hydrogen can then be converted by a fuel cell to produce electricity. In this system, batteries are used as energy buffers or for short time storage. To study the behavior of such a system, a complete model is developed by integrating individual sub-models of the fuel cell, the electrolyzer, the power conditioning units, the hydrogen storage system, and the batteries (used as an energy buffer). The sub-models are valid for transient and steady state analysis as a function of voltage, current, and temperature. A comparison between experimental measurements and simulation results is given. The model is useful for building effective algorithms for the management, control and optimization of stand-alone RESHSs.

Keywords: ARMA; Battery; Electrolyzer; Fuel cell; Photovoltaic array; Wind turbine

1. Introduction

The use of a stand-alone renewable energy system (i.e. one using wind and photovoltaic energy) in remote areas requires an energy storage device to smooth out the intermittent power input from these sources. Recent system designs [1–4] rely on batteries for short-term energy storage, while hydrogen is used for long-term energy storage. In these systems, the hydrogen (H_2) has been produced through an electrolyzer powered by the surplus energy available from the primary sources (wind turbine and photovoltaic array). When the input power is insufficient to feed the RESHS load, previously stored hydrogen is reconverted through a fuel cell (FC) to produce the required electricity. The design, management and optimization of such a system require a useful model.

We present a model to describe the dynamics of an RESHS. It integrates sub-models of the electrolyzer, the fuel cell, the batteries, the power interfaces (buck and boost converters) and the storage system. Interdependency issues (hydrogen consumption cannot exceed production) are taken into account. Special attention is given to the characterization of the system's major components in the transient state, and we use simple and realistic assumptions to describe the behavior for short- and long-term operation of the RESHS. Most of the sub-models are specified by the component's polarization curves characteristics (current–voltage–temperature). The model is validated by comparing its output to that of the Hydrogen Research Institute's (HRI) renewable energy system test bench, which is completely described in [4,6] and whose configuration and specifications are given, respectively, in Fig. 1 and Table 1. A scenario built with realistic residential power consumption needs and typical power production by wind turbine (WT), and photovoltaic (PV) array is also simulated and analyzed.

* Corresponding author. Tel.: +1 819 376 5011x3911; fax: +1 819 376 5164.
E-mail address: kodjo_agbossou@uqtr.ca (K. Agbossou).

0378-7753/$ – see front matter © 2004 Elsevier B.V. All rights reserved.
doi:10.1016/j.jpowsour.2004.08.019

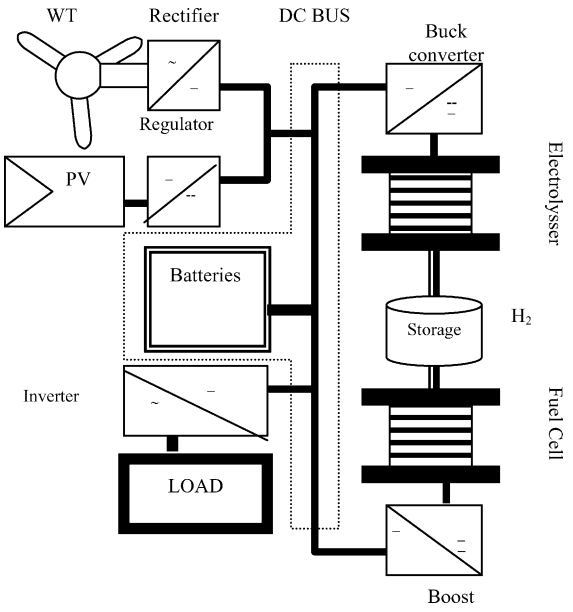

Fig. 1. Block diagram of the renewable energy system test bench of the HRI.

2. Modeling of the components

Generally, a RESHS is designed for a nominal dc bus voltage, which, in the case of the HRI test bench, is about 48 V. However, the real voltage on the dc bus depends on the operating conditions of the system. When the energy production exceeds what is needed and the battery (short-term energy storage device) is being charged, the input power devices tend to impose their output voltage on the dc bus. Wind gusts can, for example, increase that bus voltage from 48 V to 56 V in a fraction of a second. Similarly, when input energy production is below what is needed and the load draws on the battery, it is the battery that will impose its voltage on the dc bus. This variability of the bus voltage is a major control problem, as quite clearly this voltage cannot be considered as a reliable variable to describe the evolution of the state of the RESHS. Instead, it is the battery energy that will be used as a system-controlling variable (see Section 2.1).

Table 1
RE test bench technical specifications

Components	Type	Power (kW)	Voltage (V)
Photovoltaic (PV)		1	48
Wind turbine generator and regulator		10	48
Electrolyzer	Alkaline	5	26–48
Buck converter	Multiphase PWM	5	26–48
Fuel cell (FC)	PEM	5	24
Boost converter	Multiphase PWM	5	24–48
Inverter		5	110 ac
Load		0–5	110 ac
		Capacity (kWh)	
Batteries	Lead–acid	10.5–55	48
Storage H_2		125	

PWM: pulse width modulation; PEM: proton exchange membrane.

In this paper, most of the models are described as functions of time, current, voltage, and temperature. For simulation purposes, the input signals are the wind generator rectifier output current (I_{WT}), the PV array regulator output current (I_{PV}), and the load current (I_L). Due to the intermittent nature of the renewable energy sources, sampled signals will be used to represent all of them. This way, any energy production and load profile can be modeled at will. In the following sections, the models of the sub-units are presented in the order in which they are traversed by the energy flux: battery, buck converter, electrolyzer, boost converter, fuel cell, and hydrogen storage.

2.1. Battery model

The battery is the main component on the dc bus, and plays the role of an energy buffer to handle current spikes and for short-term energy storage. Different models for batteries are available, in particular those suitable for electrical vehicle applications [5,11,12,15]. For stationary applications, such as the RESHS, the models described in [2] use many experimental parameters that cannot be estimated easily, such as the overcharge effect (though in a properly-controlled RESHS, this effect does not happen, and hence is not included in the model). The main parameters, which determine the battery's performance, are its internal resistance, the polarization effect, and the long-term self-discharge rate. This self-discharge rate is difficult to estimate, and is itself subject to a number of factors, such as the operating temperature, the number of operation cycles, and the materials and technology used in its manufacture [9,14].

The battery voltage $U_B(t)$, which takes these three parameters into account is given by,

$$U_B(t) = (1 + \alpha t)U_{B,0} + R_i(t)I(t) + K_i Q_R(t) \quad (1)$$

where α is the self-discharge rate (s^{-1}); $U_{B,o}$ is the open circuit voltage (V) at $t = 0$; $R_i(t)$ is the internal resistance (Ω), K_i is the polarization coefficient ($\Omega\,h^{-1}$), and $Q_R(t)$ is the rate of accumulated ampere hours. If $I(t) > 0$ then the battery is charging; if $I(t) < 0$ then the battery is discharging. The battery energy is then,

$$W(t) = W_0 + \int_0^t P_{in}(t')\,dt' \quad (2)$$

where $P_{in}(t') = U_B(t)I(t)$ is the input power to the battery and W_0 is the battery's initial energy. As we will see later, the decision algorithm (as to whether electrolyzer or fuel cell are to be activated to rebalance the battery energy) will depend on the battery's state of charge (SOC), defined by,

$$SOC(t) = \frac{W(t)}{W_{max}} \quad (3)$$

where W_{max} is the maximum battery energy without overcharge.

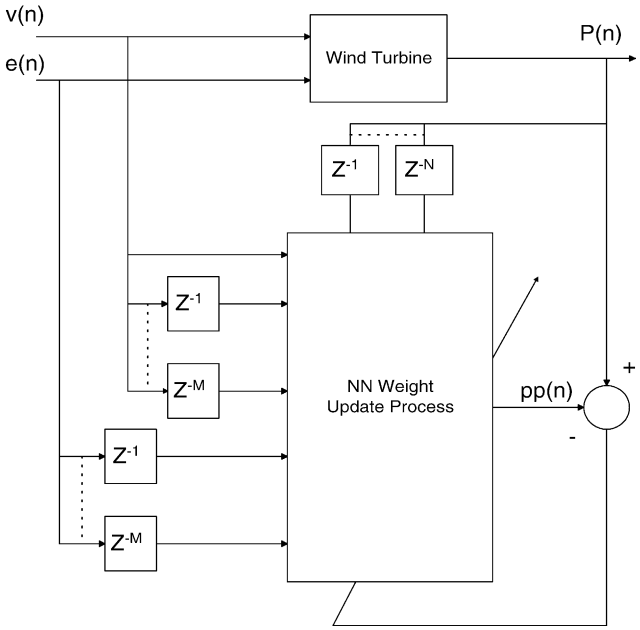

Fig. 2. Diagram of the identification process of the buck converter parameters.

2.2. Buck converter

When there is an excess of electrical energy in the system, that excess is channeled to the electrolyzer to produce hydrogen. To control this hydrogen production, a buck converter designed at HRI controls the input current to the electrolyzer cells. This buck converter is a dc voltage reducer designed to maximize the power transfer from the dc bus to the electrolyzer cells. It uses the multiphase technique to generate pulse-width modulated (PWM) signals [6]. Its models are expressed by Eqs. (4) and (5), and they give the voltage and current applied to the electrolyzer cells. Considering the complexity of describing these circuits, an autoregressive moving average (ARMA) model (Fig. 2) [16] for parameter identification is used to minimize the average quadratic error between the real output of the buck converter and the model's. During this process, the time scale is set to 1 s and the buck converter operating temperature to 25 °C.

The following equation (based on the ARMA model) gives the relation between the buck output voltage and the dc bus voltage (transfer function),

$$U_{\mathrm{Bu,Out}}(n) = U_{\mathrm{B}}(n)\frac{\left(B_{\mathrm{Bu},0} + B_{\mathrm{Bu},1}z^{-1}\right) D_{\mathrm{Bu}}(n)}{A_{\mathrm{Bu},0} + A_{\mathrm{Bu},1}z^{-1}} \tag{4}$$

where $A_{\mathrm{Bu},0}$, $A_{\mathrm{Bu},1}$, $B_{\mathrm{Bu},0}$, and $B_{\mathrm{Bu},1}$ are parameters which have to be determined. Their values, for our case, are given in Table 2. U_{B} is the dc bus voltage; D_{Bu} is the duty cycle and $U_{\mathrm{Bu,Out}}$ is the buck converter output voltage (and applied to the electrolyzer cells). The buck converter input voltage ($U_{\mathrm{Bu,In}}$) is equal to the dc bus voltage because of its direct connection to the dc bus. Taking into account the buck power efficiency (η_{Bu}), the input current ($I_{\mathrm{Bu,In}}$) to the buck converter is

Table 2
Parameter values

Component	Parameters	Values
Battery	R_{i} (Ω)	0.076
	K_{i}	∼0
	Q_{FC} (A h)	880
	Q_0 (A h)	880
	E_0 (V)	48
Boost converter	$A_{\mathrm{Bo,o}}$	1
	$A_{\mathrm{Bo,I}}$	−0.2045
	$B_{\mathrm{Bo,o}}$	1.236
	$B_{\mathrm{Bo,I}}$	−0.4275
Buck converter	$A_{\mathrm{Bu,o}}$	1
	$A_{\mathrm{Bu,I}}$	−1.485
	$\eta_{\mathrm{I,el}}$	0.7
	$B_{\mathrm{Bu,o}}$	0.057
	$B_{\mathrm{Bu,I}}$	−0.082
Electrolyzer	$U_{\mathrm{el},0}$	22.25
	C_1	−0.1765
	C_2	5.5015
	$\eta_{\mathrm{I,FC}}$	0.45
	$I_{\mathrm{el},0}$	0.1341
	R_{el}	−3.3189
	$N_{\mathrm{Cell,el}}$	24
PEMFC	U_{FC}	33.18
	E_1	−0.013
	E_2	−1.57
	$I_{\mathrm{FC},0}$	8.798
	R_{FC}	−2.04
	$N_{\mathrm{Cell,FC}}$	35

$$I_{\mathrm{Bu,In}}(n) = \frac{U_{\mathrm{Bu,Out}}(n) I_{\mathrm{Bu,Out}}(n)}{\eta_{\mathrm{Bu}} U_{\mathrm{Bu,In}}(n)} \tag{5}$$

where $I_{\mathrm{Bu,Out}}$ is the input current to the electrolyzer cells, and is determined in the next section. The coefficients may vary slightly from one operating point to another, but on the whole, the model gives a good account of the dynamics of the system.

2.3. Electrolyzer

As the electrolyzer time response is slow [10] compared to the modeling sampling time (1 s), the output voltage is given by,

$$U_{\mathrm{el}}(t) = U_{\mathrm{el},0} + C_1 T_{\mathrm{el}}(t) + C_2 \ln\left(\frac{I_{\mathrm{el}}(t)}{I_{\mathrm{el},0}}\right) + \frac{R_{\mathrm{el}}}{T_{\mathrm{el}}(t)} I_{\mathrm{el}}(t) \tag{6}$$

where $U_{\mathrm{el},0}$ (V), C_1 (V °C^{-1}), C_2 (V °C^{-1}), $I_{\mathrm{el},0}$ (A) and R_{el} (Ω °C^{-1}) are parameters to be determined experimentally. For the HRI test bench, their values are given in Table 2 for an operating temperature $T_{\mathrm{el}}(t)$ between 22 °C and 52 °C. The first two terms of Eq. (6) represent the theoretical potential of an ideal cell. The third term gives the activation potential, while the last one represents resistance (ohmic) losses. These parameter values vary from one electrolyzer to another. Con-

sidering that the output of the buck converter is connected directly to the input of the electrolyzer cells, $U_{\mathrm{Bu,Out}}(t)$ and $I_{\mathrm{Bu,Out}}(t)$ are equivalent to $U_{\mathrm{el}}(t)$ and $I_{\mathrm{el}}(t)$, respectively. The hydrogen production rate $\dot{V}_{\mathrm{el}}(t)$ is given by,

$$\dot{V}_{\mathrm{el}} = N_{\mathrm{Cell,el}} \frac{\eta_{\mathrm{I,el}} I_{\mathrm{el}}(t)}{C_{\mathrm{H_2}}} \tag{7}$$

where $\eta_{\mathrm{I,el}}$ is the electrolyzer utilization factor; $N_{\mathrm{Cell,el}}$ represents the number of cells, and $C_{\mathrm{H_2}}$ is a conversion coefficient (of value 2.39 A h l^{-1} of hydrogen). $\eta_{\mathrm{I,el}}$ depends on the cell temperature. For alkaline electrolyzers, some studies [7,8,13] show that $\eta_{\mathrm{I,el}}$ is between 0.6 and 0.75. A more rigorous estimate can be obtained by direct measurement of the production. The hydrogen produced by the electrolyzer is stored, and can be used later by the FC. The storage sub-system model is given in Section 2.5.

2.4. Boost converter

The nominal output voltage of HRI's fuel cell is around 24 V, whereas the dc bus is designed for 48 V. Hence a power interface is necessary between the two. In order to maximize the power transfer between the FC and the dc bus the boost converter is designed with the same multiphase switching technique and pulse-width modulated signals, as was used for the buck converter. Using the same method as described in Section 2.2, the relation between the duty cycle D_{Bo} and the input current $I_{\mathrm{Bo,In}}(t)$ of the boost converter is given by,

$$I_{\mathrm{Bo,In}}(n) = I_{\mathrm{FC,Max}} \frac{\left(B_{\mathrm{Bo},0} + B_{\mathrm{Bo},1} z^{-1}\right) D_{\mathrm{Bo}}(n)}{A_{\mathrm{Bo},0} + A_{\mathrm{Bo},1} z^{-1}} \tag{8}$$

where $I_{\mathrm{FC,Max}}$ is the maximum output current of the FC; $A_{\mathrm{Bo},0}$, $A_{\mathrm{Bo},1}$, $B_{\mathrm{Bo},0}$, and $B_{\mathrm{Bo},1}$ are parameters to be determined (see Table 2). The output current ($I_{\mathrm{Bo,Out}}$) of the boost converter is obtained from the boost power efficiency (η_{Bo})

$$I_{\mathrm{Bo,Out}}(n) = \eta_{\mathrm{Bo}} \frac{U_{\mathrm{FC}}(n) I_{\mathrm{Bo,In}}(n)}{U_{\mathrm{B}}(n)} \tag{9}$$

where U_{FC} is the FC output voltage, and η_{Bo} is determined by direct measurement (and found to be >95%).

2.5. Proton exchange membrane fuel cell

According to references [6–8], the proton exchange membrane (PEM) FC reaction time constants during transient periods (<50 ms) are smaller than the simulation step time (1 s). Hence, the dynamic behavior of the FC is given by its polarization curve

$$U_{\mathrm{FC}}(t) = U_{\mathrm{FC},0} + E_1 T_{\mathrm{FC}}(t) + E_2 \ln\left(\frac{I_{\mathrm{FC}}(t)}{I_{\mathrm{FC},0}}\right) + \frac{R_{\mathrm{FC}}}{T_{\mathrm{FC}}(t)} I_{\mathrm{FC}}(t) \tag{10}$$

where $U_{\mathrm{FC},0}$ (V), E_1 (V °C^{-1}), E_2 (V °C^{-1}), $I_{\mathrm{FC},0}$ (A), and R_{FC} (Ω °C^{-1}) are experimental parameters whose values as measured on the IRH test bench are given in Table 2 for temperatures ranging from 24 °C to 72 °C. $T_{\mathrm{FC}}(t)$ is the operating temperature of the cells, which changes during the cell's operation. The first two terms of Eq. (10) represent the open loop potential, the third term corresponds to the activation potential, and the last represents resistance (ohmic) losses. These parameters vary widely from one fuel cell to another. The FC's hydrogen consumption rate $\dot{V}_{\mathrm{FC}}(t)$ is given by,

$$\dot{V}_{\mathrm{FC}} = N_{\mathrm{Cell,FC}} \frac{\eta_{\mathrm{I,FC}} I_{\mathrm{FC}}(t)}{C_{\mathrm{H_2}}} \tag{11}$$

where $\eta_{\mathrm{I,FC}}$ is the utilization factor of the FC, and $N_{\mathrm{Cell,FC}}$ represents the number of cells. The literature [7,8] shows that $\eta_{\mathrm{I,FC}}$ is between 0.3 and 0.6 for PEM fuel cells. A more accurate estimate can be obtained by direct measurement.

2.6. Hydrogen storage sub-system

The hydrogen produced by the electrolyzer is stored in a pressurized tank. Although the actual renewable energy system at HRI has a compressor and the hydrogen can be stored in a tank at up to 150 psi, the equations used will assume hydrogen storage at normal pressures and temperatures. The power balance for the storage function is given by

$$\frac{\mathrm{d}W_{\mathrm{H_2}}(t)}{\mathrm{d}t} = P_{\mathrm{el}}(t) - P_{\mathrm{FC}}(t) \tag{12}$$

where $W_{\mathrm{H_2}}(t)$ is the energy present in the tank in the form of hydrogen, $P_{\mathrm{FC}}(t)$ and $P_{\mathrm{el}}(t)$ are, respectively, the FC power consumption (related to the H_2 consumption rate) and the electrolyzer power production (related to the H_2 production rate). The solution of Eq. (12) in the Laplace domain is given by

$$W_{\mathrm{H_2}}(s) = \frac{P_{\mathrm{el}}(s) - P_{\mathrm{FC}}(s)}{s} + W_{\mathrm{H_{2,0}}} \tag{13}$$

with

$$P_{\mathrm{el}}(s) = \frac{\dot{V}_{\mathrm{el}}(s)}{V_{\mathrm{T}}} \Delta H; \qquad P_{\mathrm{FC}}(s) = \frac{\dot{V}_{\mathrm{FC}}(s)}{V_{\mathrm{T}}} \Delta H$$

where $\dot{V}_{\mathrm{el}}$ and $\dot{V}_{\mathrm{FC}}$ are, respectively, the production and the consumption rates of H_2. $W_{\mathrm{H_{2,0}}}$ is the initial hydrogen energy stored. Under normal temperature and pressure conditions [9], V_{T} is equal to 22.4 l mol^{-1}. ΔH is the enthalpy of hydrogen ("high heating value") (ΔH = 286 kJ mol^{-1}).

3. RESHS simulation

A model of a RESHS has been developed based on the above equations for its sub-units. The simulation block diagram is given in Fig. 3. As mentioned earlier, the simulation and sampling time step is taken as 1 s, and N is the total number of steps for one complete operation period. The principal results of interest are the output currents of the buck converter

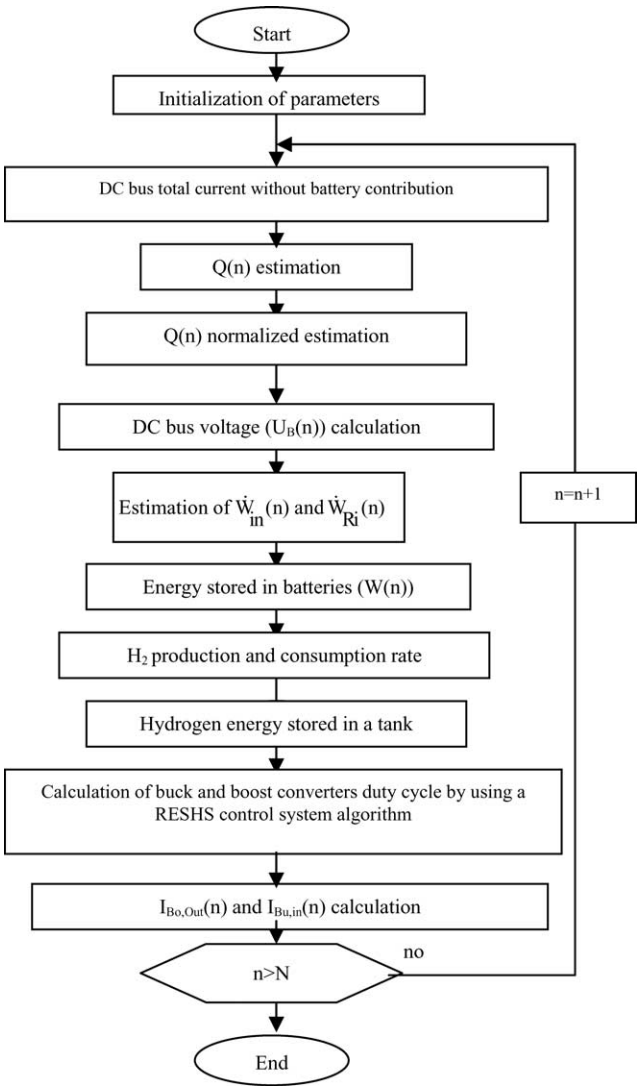

Fig. 3. RESHS simulation block diagram.

and of the boost converter, and the energy stored in the battery. The boost converter output current depends of course on the details of the models of the boost converter and of the FC. Similarly, the electrolyzer current is closely associated with the details of the buck converter and of the electrolyzer. In this diagram, $Q(n)$ represents the accumulated ampere hours in batteries.

4. Experimental and performance analysis

The models of the sub-units described previously were used to put the RESHS system through a typical run (the values of the parameters of the various sub-units are found in Table 2). In order to reflect the variable nature of the actual WT and PV array power variations, the simulation inputs were subjected to relatively large ripples, and the simulation outputs were monitored closely to determine the stability of the model. The simulation inputs are the WT generator current at the dc bus (I_{WT}), the PV array regulator current (I_{PV}), the load current (I_L), the electrolyzer cell temperature (T_{el}) (which is relatively constant: 25 °C) and the FC cell temperature (T_{FC}), which varies linearly from 25 °C to 35 °C with a slope of 3.3 °C s^{-1}. The simulation outputs are (as mentioned previously) the buck converter output current (same as the electrolyzer input current) (I_{el}), the boost converter output current ($I_{Bo,Out}$), and the battery energy ($W(t)$). All these signals were also measured on the actual HRI operating test bench to permit comparison of the simulation output with reality.

The electrolyzer and FC regulators work so as to bring the battery energy $W(t)$ back towards its reference value, W_{ref}, whenever $W(t)$ gets beyond a pre-determined range bounded by W_{hi} and W_{low} bracketing W_{ref}. The electrolyzer, which lowers $W(t)$ by converting the excess battery energy into hydrogen (i.e. when the input energy is greater than what is needed by the load), is powered on when $W(t) > W_{hi}$, and is stopped when W_{ref} is reached. The FC, which raises $W(t)$ by converting hydrogen back into battery energy (i.e. when the input energy is smaller than what is needed by the load), is powered on when $W(t) < W_{low}$, and is stopped again when W_{ref} is reached. The system starts with an initial energy $W_0 > W_{hi}$ (W_0 is estimated to 42,240 Wh), usually at W_{hi}. In the first simulation W_{ref} = 42,218 Wh, and W_{hi} and W_{low} are at 42,240 Wh (=W_{ref} + 22 Wh) and 42,196 Wh (=W_{ref} − 22 Wh). The control range thus extends to ±22 Wh around W_{ref}.

4.1. Input signals

Figs. 4 and 5 present typical WT output and load current (two of the simulation input variables). It can be noticed that the system operates during 7 min. There was no significant power available from PV array when running this experience.

4.2. Electrolyzer

The electrolyzer, which is fed from the buck converter, is set to operate at a nominal input power of 1500 W when it is

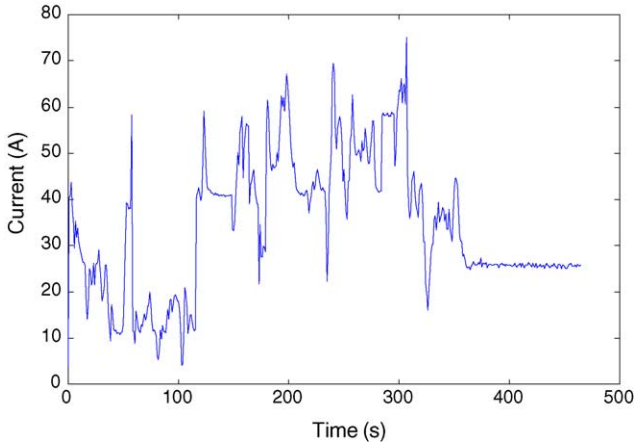

Fig. 4. Current $I_{WT}(t)$ from the wind turbine through the rectifier module.

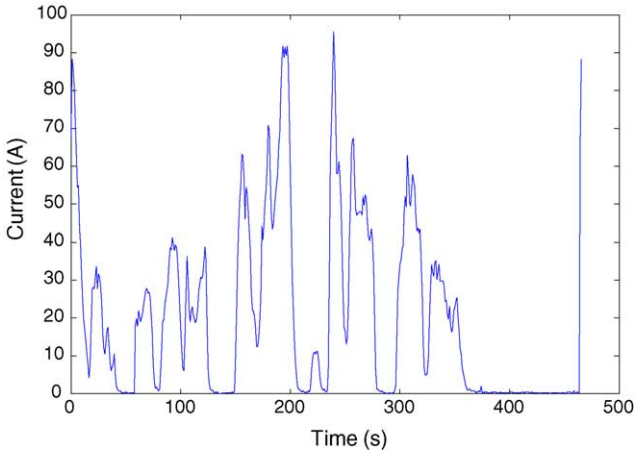

Fig. 5. Profile of the load current.

running. When the simulation starts, the electrolyzer is operating according to the control strategy described above. Fig. 6 compares the experimental and the simulation results. The difference between simulation and measurements is around 8.5%. This result shows that the models of the buck converter and the electrolyzer are relatively realistic. The steady-state difference between the two (at $t > 65$ s) is due to the inaccurate estimation of the initial energy of the battery (W_0) in Eq. (2) (it turns out that the model of the energy buffer is itself dependent on the initial energy stored in the battery). In spite of this, the start–stop sequences of the electrolyzer are the same for the simulation and the experimental measurements.

4.3. Fuel cell

For the FC and the boost converter, the simulated and experimental (measured) currents are perfectly matched (Fig. 7). The deviation between the two is less than 2%. It turns out that the boost converter output current is not very sensitive to reasonable variations of the dc bus voltage.

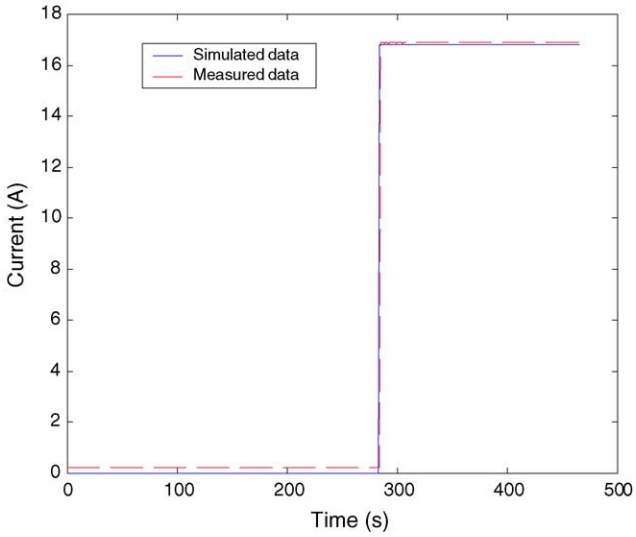

Fig. 7. Comparison of the simulated and measured current of the boost converter output.

4.4. Buffer energy

The overall quality of the simulation of the operation of the RESHS is judged by examining the time-evolution of the buffer energy ($W(t)$). Fig. 8 gives the measured and simulated results. From $t = 0$ s to $t = 65$ s, $W(t)$ decreases quickly, because (1) insufficient energy is available from the wind turbine and the PV array (see Figs. 4 and 5), and (2) the electrolyzer is running and withdrawing energy from the battery (Fig. 6).

When $W(t)$ reaches W_{ref} at $t = 66$ s, the control program shuts the electrolyzer off. $W(t)$ then starts to rise (from $t = 66$ s to $t = 135$ s). Figs. 4 and 5 show that there is a surplus

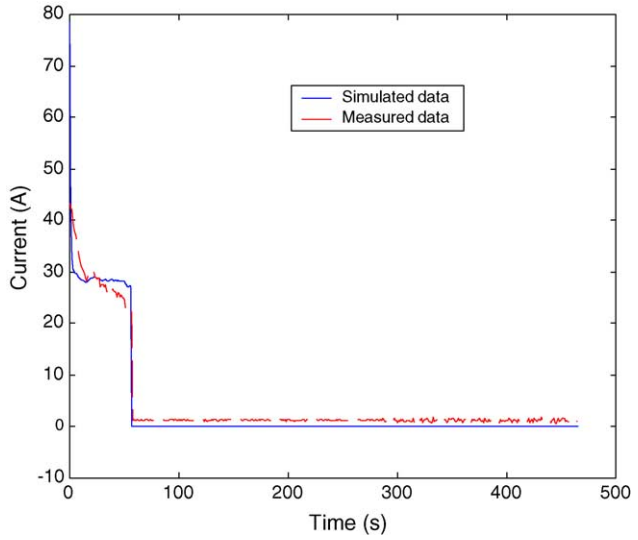

Fig. 6. Comparison of the electrolyzer current simulated and measured.

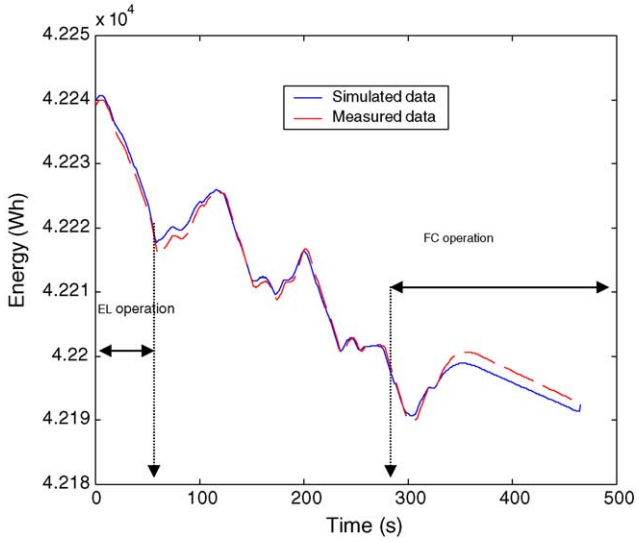

Fig. 8. Battery energy $W(t)$.

power on the dc bus during this period, and this surplus is transferred into the battery. From t = 136 s to t = 200 s, $W(t)$ decreases again due to the high load current (Fig. 5) and the insufficient energy supply from the wind turbine. At t = 295 s, $W(t)$ reaches the threshold value W_{low} at which the control program turns the FC on (Fig. 7), to supply the required energy from the stored hydrogen. Beyond t = 350 s, the WT current is essentially zero, while the load current remains at about 25 A and the FC current at only 17 A, and hence $W(t)$ decreases again due to the net 8 A drawn from the battery. The difference between the simulated and the measured $W(t)$ seems to be less than 2%. This is a good indication of the reliability of the models.

5. Residential energy consumption scenario

A realistic scenario of the energy consumption of a residence is now developed. The values used for the power productions of the PV array and of the wind turbine are typical for our region. The net dc bus power, that is the algebraic sum of powers from the PV array, the wind turbine, and the load (this one negative) but without the contribution of the FC and of the electrolyzer is shown in Fig. 9. It stays, on the average, negative until t = 3800 s, and slightly positive afterwards. Positive power values mean that excess power is available at the dc bus, while negative power values means that there is a power deficit at the bus. The simulation of this scenario covers 2 h (7200 s).

The electrolyzer and FC model parameters are again given in Table 2, while their on/off control criteria are similar to the previous simulation. The target value W_{ref} is $0.70W_0$. The electrolyzer is started when $W(t) > 0.75W_{max}$ and stopped when $W(t) < 0.70W_{max}$. The FC is started when $W(t) < 0.65W_{max}$ and stopped when $W(t) > 0.70W_{max}$. The maximum capacity of the battery (W_{max}) is set at 11 kWh. The initial battery charge (W_0) is set at 0.75 W_{max}.

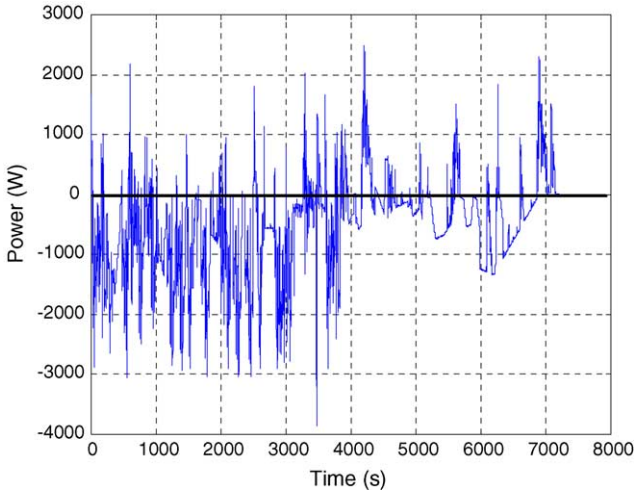

Fig. 9. Net power on the dc bus without the contributions of FC and electrolyzer.

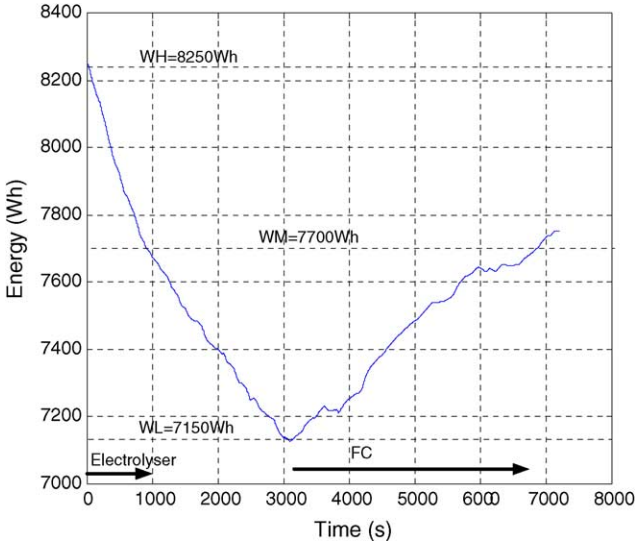

Fig. 10. Battery energy $W(t)$: $W_{hi} = 0.75W_{max}$, $W_{ref} = 0.70W_{max}$, $W_{low} = 0.65W_{max}$.

The evolution of $W(t)$ is displayed in Fig. 10. When the system starts (t = 0 s), $W(t)$ is at $0.75W_{max}$, and the electrolyzer is running (Fig. 11). The battery energy $W(t)$ decreases (see Fig. 10) because, again, the net power (Fig. 9) is negative (the consumption is more than the energy production) and because the electrolyzer is also running. At t = 990 s, $W(t)$ reaches $W_{ref} = 0.7W_{max}$ (Fig. 10), and the control algorithm stops the electrolyzer (Fig. 11). From t = 991 s to t = 2995 s, neither the FC nor the electrolyzer are operating (Fig. 11), and $W(t)$ keeps decreasing, since the net power on the dc bus is negative during this period (Fig. 9). $W(t)$ keeps decreasing until, at t = 2995 s, it reaches the value of $W_{low} = 0.65W_{max}$, at which point the control logic turns the FC on, and energy flows back into the battery from the converted hydrogen. The FC is operating from then until 6900 s (Figs. 10 and 11), at

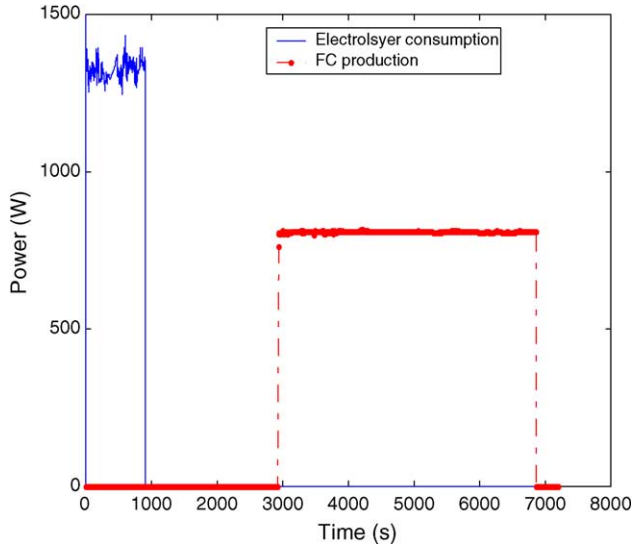

Fig. 11. Power of the electrolyzer and the FC.

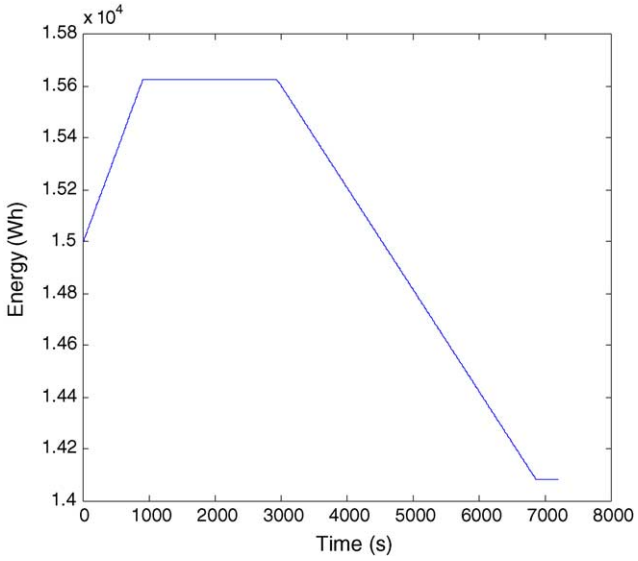

Fig. 12. Energy of the stored hydrogen $W_{H_2}(t)$.

which point $W(t)$ reaches W_{ref} again and the FC is turned off.

Fig. 12 shows the equivalent evolution of the energy of the stored hydrogen. The initial stored energy ($W_{H_{2,0}}$) is set to 15 kWh. It is obvious that when the electrolyzer is in operation producing hydrogen ($0 < t < 991$ s), $W_{H_2}(t)$ increases, and when the FC works consuming hydrogen ($t > 2990$ s), $W_{H_2}(t)$ decreases.

These results show that the models described in this paper can be used to predict the performance of a renewable energy system with hydrogen storage for any reasonable scenario. Moreover it is possible to know the conditions necessary to make the system autonomous by checking the hydrogen sufficiency in the system (Fig. 12). The stored amount of hydrogen energy gives us the time during which the RESHS could work as a purely stand-alone source in the extreme case of zero power input from the WT or the PV array.

6. Conclusions

We developed a model to simulate a power generator fed by renewable energies (wind and light), with batteries and gaseous hydrogen as energy reservoirs, and electrolyzers and fuel cells as converters of energy between electrical and hydrogen. Special attention has been given to the modeling of each sub-unit of the system. The electrolyzer and the fuel cell are modeled by using their steady-state polarization curves. Due to the important role of power interfaces (boost and buck converters) in the RESHS, they are modeled for both their transient and steady state behaviors (ARMA model). A simplified model is used for the battery, with parameters easy to estimate, and tested with all the other system components. The validation of all component models is based on a 10-stage algorithm that develops their dynamic evolution during the course of the simulation. Comparison with experimental data confirms that these models give realistic and reliable results. The simulation gives an average deviation estimated at less than 5% compared to an actual test-bench generator, even in the presence of strong fluctuations of the primary energy input sources. A second application of the model was to simulate the power scenario for a residential application, with power sources typical for our region. The results confirm again that the model can describe the behavior of a RESHS in a realistic way.

Acknowledgements

This work has been supported in part by the Natural Sciences and Engineering Research Council of Canada, the Ministère de la Recherche, de la Science et de la Technologie du Québec, and the Canada Foundation for Innovation.

References

[1] K. Agbossou, R. Chahine, J. Hamelin, F. Laurencelle, A. Anouar, J.-M. St-Arnaud, T.K. Bose, J. Power Sources 96 (2001) 168–172.
[2] S.R. Vosen, J.O. Keller, Int. J. Hydrogen Energy 24 (1999) 1139–1156.
[3] A.G. Dutton, J.A.M. Bleijs, H. Dienhart, M. Falchetta, W. Hug, D. Prischich, A.J. Ruddell, Int. J. Hydrogen 25 (2000) 705–722.
[4] K. Agbossou, M. Kolhe, J. Hamelin, É. Bernier, T.K. Bose, Int. J. Renewable Energy 28 (8) (2004) 1305–1318.
[5] L.E. Unnewehr, S.A. Nsar, Electric Vehicle Technology, John Wiley, 1982, pp. 81–91.
[6] K. Agbossou, R. Simard, S. Kelouwani, T.K. Bose, CCECE'2001: Proceedings of the IEEE Canadian Conference on Electrical and Computer Engineering, Toronto, Canada, Paper 178, 2001.
[7] J.P. Vanhanen, P.D. Lund, Int. J. Hydrogen Energy 20 (7) (1995) 575–585.
[8] W. Hug, H. Bussmann, A. Brinner, Int. J. Hydrogen Energy 18 (1993) 973–977.
[9] D. Linden, Handbook of Batteries, McGraw-Hill, USA, 1994.
[10] P.S. Kauranen, P.D. Lund, J.P. Vanhanen, Int. Assoc. Hydrogen Energy 19 (1) (1994) 99–106.
[11] L. Barra, D. Coiante, Int. Assoc. Hydrogen Energy 18 (8) (1993) 685–693.
[12] Y. Kim, S. Kim, IEEE Transact Energy Conversion 14 (2) (1999) 239–244.
[13] F. Laurencelle, R. Chahine, J. Hamelin, K. Agbossou, M. Fournier, T.K. Bose, Fuel Cells 1 (1) (2001) 66–71.
[14] http://www.radtherm.com/support/publications/batterymodelsdoc.html.
[15] P. Mauracher, E. Karden, K. Rembe, Proceedings of the International Conference on Lead–Acid Batteries LABAT'96, 1996.
[16] C. Alippi, V. Piuri, IEEE Transact. Instrum. Meas. 45 (2) (1996) 670–676.